



HAL
open science

Multipixel x ray detection integrated at the end of a narrow multicore fiber

Carlos Chacon, Miguel Suarez, Vahe Karakhanyan, Kewin Desjardin, Claude Menneglier, Olivier Soppera, Virginie Moutarlier, Thierry Grosjean

► **To cite this version:**

Carlos Chacon, Miguel Suarez, Vahe Karakhanyan, Kewin Desjardin, Claude Menneglier, et al.. Multipixel x ray detection integrated at the end of a narrow multicore fiber. *Optics Letters*, 2023, 48 (8), pp.2178-2181. 10.1364/OL.484887. hal-04261364v2

HAL Id: hal-04261364

<https://hal.science/hal-04261364v2>

Submitted on 27 Oct 2023

HAL is a multi-disciplinary open access archive for the deposit and dissemination of scientific research documents, whether they are published or not. The documents may come from teaching and research institutions in France or abroad, or from public or private research centers.

L'archive ouverte pluridisciplinaire **HAL**, est destinée au dépôt et à la diffusion de documents scientifiques de niveau recherche, publiés ou non, émanant des établissements d'enseignement et de recherche français ou étrangers, des laboratoires publics ou privés.

Multi-pixel X-ray detection integrated at the end of a narrow multicore fiber

CARLOS CHACON¹, MIGUEL SUAREZ¹, VAHE KARAKHANYAN¹, KEWIN DESJARDIN², CLAUDE MENNEGLIER², OLIVIER SOPPERA^{3,4}, VIRGINIE MOUTARLIER⁵, AND THIERRY GROSJEAN^{*,2}

¹FEMTO-ST Institute - CNRS UMR 6174 - University of Bourgogne Franche-Comte, Besançon, France

²Synchrotron SOLEIL, Saint-Aubin, 91192 Gif-sur-Yvette, France

³Université de Haute-Alsace, CNRS, IS2M UMR 7361, F-68100 Mulhouse, France

⁴Université de Strasbourg, 67000 Strasbourg, France

⁵UTINAM Institute - CNRS UMR 6213 - University of Bourgogne Franche-Comte, Besançon, France

* Corresponding author: thierry.grosjean@univ-fcomte.fr

Compiled December 23, 2022

We introduce and demonstrate the concept of a multi-pixel detector integrated at the tip of an individual multicore fiber. A pixel consists here of an aluminum-coated polymer microtip incorporating a scintillating powder. Upon irradiation, the luminescence released by the scintillators is efficiently transferred into the fiber cores owing to the specifically elongated metal-coated tips which ensure efficient luminescence matching to the fiber modes. Each pixel being selectively coupled to one of the cores of the multicore optical fiber, the resulting fiber-integrated X-ray detection process is totally free from inter-pixel cross-talk. Our approach holds promise of fiber-integrated probes and cameras for remote X- and Gamma-ray analysis and imaging in hard-to-reach environments. © 2022 Optica Publishing Group

<http://dx.doi.org/10.1364/ao.XX.XXXXXX>

The need for novel tools able to detect ionizing radiations within tiny recesses and/or extreme environments (of high pressure, temperature or radioactivity) is seen to rapidly grow in many scientific, medical and industrial domains. Being compact, robust and flexible, optical fibers are widely considered as a promising optical tool for addressing this demand, as they allow a direct control on light encoded information collected from hard-to-reach locations.

Fiber probes based on the integration of a scintillating element onto the tip of the optical fiber have been widely explored for the local and real-time dosimetry of ionizing radiations. Given their inert, passive, and possibly biocompatible nature, such devices are particularly appealing in a variety of applications and techniques ranging from in-vivo dosimetry in cancer therapies to *in situ* dosimetry within harsh environments such as a nuclear reactor [1–8].

Most of these studies have been realized with single pixel detectors obtained by coupling a scintillating cell to an individual fiber. Bringing multi-pixel X-ray detectors within hard-to-reach environments would enable new opportunities in radiation analysis, opening the prospect of *in vivo* or *in situ* real-time imaging.

However, integrating a pixel array in a compact fiber-integrated architecture remains a challenge. Optical fibers being typically larger than 90 μm , the parallel implementation of a single pixel fiber probe in a fiber bundle represents limits in terms of compactness and image sampling [9].

Compactness and resolution issues can be alleviated by implementing multiple pixels onto the same optical fiber. Therriault et al. developed a three-pixel detector integrated at the end of an individual fiber [10]. The multi-pixel probe was sufficiently compact to be inserted within a catheter for brachytherapy applications [11, 12]. However, since the luminescence spectra of the three different scintillators used as detection pixels noticeably overlap, the detector suffers from inter-pixel cross-talk. The development of an array of detection pixels at the tip of an individual optical fiber has so far never been reported.

In this paper, we demonstrate a seven-pixel X-ray detector engineered at the tip of an individual fiber. Our detector is achieved by coupling seven metal-coated scintillating micro-tips to a multicore fiber, each microtip being coupled to one of the fiber cores. The resulting seven parallel detection channels are shown to be totally independent from each other, thus holding promise for a high contrast real-time imaging in hard-to-reach environment. Demonstration is realized both with monochromatic and polychromatic X-rays. Multicore fibers have recently demonstrated new prospects for sensing applications [13, 14] and lab-on-fiber technology [15, 16]. We here extend the multicore-fiber-based technology to the analysis and imaging from ionizing radiations.

Our fiber-integrated multipixel detection system is fabricated using a photopolymerization process at one endface of a multicore fiber from Fibercore (Model SM-7C1500). The optical fiber shows seven 6.3- μm -diameter cores arranged in a hexagonal lattice, with an inter-core spacing of 35 μm . The photopolymerization involves a scintillating photopolymer locally exposed with a laser light travelling through the fiber. One fiber endface is immersed with the polymer/scintillator mixture while an expanded laser beam ($\lambda=521$ nm, laser diode from Thorlabs) is projected onto the other end to homogeneously illuminate all the cores of the fiber. The so-excited seven parallel

64 fiber modes carry almost the same power, thereby similarly trig- 98
 65 gering polymer hardening at the core outputs. The total laser 99
 66 power at the fiber output and exposure time are $0.7 \mu\text{W}$ and 4 100
 67 seconds, respectively. After fiber rinsing with ethanol, seven 101
 68 scintillating microtips arranged in a hexagonal lattice appear 102
 69 at the fiber output face. Being realized from the fiber modes 103
 70 themselves at a wavelength closely approaching that of the scin- 104
 71 tillator luminescence, the so-produced elongated scintillating 105
 72 microtips are expected to reciprocally efficiently transfer their 106
 73 X-ray excited luminescence into the fiber. To increase probe effi- 107
 74 ciency, the multipixel detection array can be metal coated to limit 108
 75 the luminescence leaving the microtips outside the fiber. Metal 109
 76 coating involves here the deposition of a few-nanometer-thick 110
 77 titanium adhesion layer followed by a 125-nm thick aluminum 111
 78 layer. Aluminum is chosen for its high reflectivity at visible 112
 79 wavelengths and high transparency to X-rays.

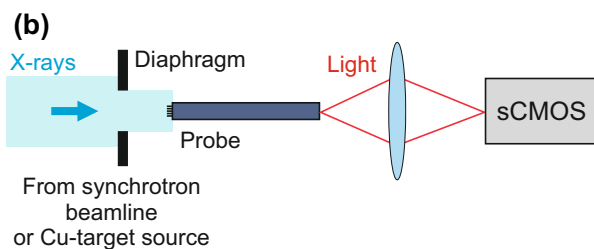
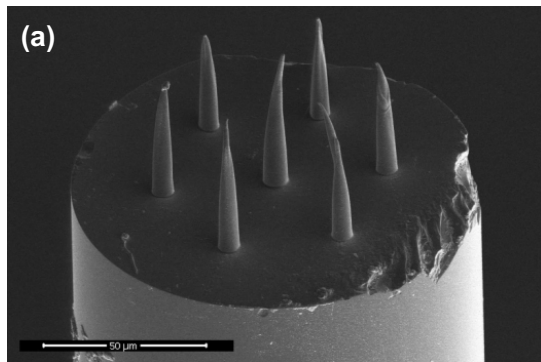


Fig. 1. (a) SEM image of a fiber-integrated multi-pixel detection array on top of a seven-core optical fiber. Each pixel is in direct optical coupling with one of the fiber core. (b) Scheme of the experimental set-up for the detector demonstration.

80 To produce the scintillating photopolymer, we first grind 143
 81 a commercial $\text{Gd}_2\text{O}_2\text{S:Eu}$ powder (Phosphor Technology, 144
 82 Ref.UKL63/UF-R1) in a mortar with a pestle. The ground powder 145
 83 is then mixed with ethanol to be filtered with a cellulose 146
 84 acetate membrane whose pore diameter is of $1.2 \mu\text{m}$. Finally, the 147
 85 filtrate is dried to form a superfine powder. Next, the scintil- 148
 86 lating material is mixed with a photosensitive polymer, which 149
 87 combines an eosin Y (tetrabromofluorescein) used as a sensi- 150
 88 tizer dye, an co-initiator (MDEA: N-methyldiethanola-mine) 151
 89 and a multifunctional acrylate monomer, pentaerytritoltriacy- 152
 90 late (PETIA) [17]. This photosensitive emulsion provides robust 153
 91 microstructures at the endface of an optical fiber [18–21]. A 154
 92 weight ratio of 1:5.2 between the photopolymer and the scintil- 155
 93 lating powder ensures a high concentration of scintillator within 156
 94 the mixture. $\text{Gd}_2\text{O}_2\text{S:Eu}$ shows excellent yield, linearity and 157
 95 stability upon exposure [21, 22]. This scintillator also show 158
 96 sub-millisecond decay and low afterglow upon exposure at energies 159
 97 of the order of a few keV, thereby leading to a response time that 160

is fast enough for numerous applications. Faster luminescence 161
 may however be achieved with $\text{Gd}_2\text{O}_2\text{S:Tb}$ material [6, 23, 24].

Figure 1(a) displays a scanning electron micrograph of a re- 162
 sulting fiber-integrated multipixel detector. The pixel array takes 163
 the form of seven aluminum-coated scintillating micro-tips of 164
 similar geometries located on top of the seven fiber cores.

The microfabricated detector is demonstrated at the Metrol- 165
 ogy beamline of the synchrotron Soleil. The experimental set-up 166
 is depicted in Fig. 1(b). A monochromatic 12-keV radiation is 167
 projected onto the microstructured facet of the fiber (the beam 168
 and fiber axes are aligned). At 12 keV, a flux of $2.1 \cdot 10^9$ photons/s 169
 is measured across the $1 \times 1 \text{mm}^2$ radiation field. An adjustable 170
 diaphragm is positioned in front of the fiber, to control the beam 171
 width. The diaphragm and fiber detector are positioned on two 172
 independent 3D motorized stages. The bare output face of the 173
 fiber is imaged with a standard sCMOS camera (Zyla model 174
 from Andor Technology) equipped with a ($\times 10, 0.3$) microscope 175
 objective (Olympus). The camera is positioned outside the irradi- 176
 ation zone of the primary beam. We verified that negligible stem 177
 effect (i.e., Cerenkov effect) [25, 26] is generated by the fiber itself 178
 upon exposure: no signal is detected when a bare scintillator-free 179
 multicore fiber is placed within the above-described test-bed. 180
 The camera is used as a photometer array to simultaneously 181
 read the seven instant optical signals delivered in parallel by 182
 the fiber-integrated multipixel platform. The readout signals are 183
 obtained by integrating image intensity over 64×64 -pixel regions 184
 of interest (ROI) tightly enclosing the seven output light spots 185
 (one ROI per spot). Images are recorded at a rate of 10 Hz.

Figure 2(a) shows an image of the output endface of the multi- 186
 core fiber. The observed seven light spots originate from the scin- 187
 tillation light generated upon irradiation by the fiber-integrated 188
 pixel array and guided through the fiber to the camera. These 189
 light spots are well separated in the image, thereby avoiding arti- 190
 factual inter-pixel crosstalk in the optical readout process. Since 191
 a relatively homogeneous distribution of light spots is imaged 192
 by the camera (see Fig. 2(b)), we conclude that the concentration 193
 of scintillators across the microtip array is almost constant and 194
 the fabrication process satisfies pixel homogeneity. Only one 195
 pixel shows a signal level deviating from the others's. Note that 196
 correction factors can be applied to the pixel array to correct 197
 little signal offsets.

The response of our fiber-integrated multipixel detector in 198
 terms of dose linearity and repeatability is reported in Fig. 3. 199
 The measurement repeatability (Fig. 3(a)) is determined over 200
 ten exposures of ten seconds each. For the ten exposures at a 201
 near-constant radiation flux, the light intensities accumulated 202
 by each detection pixel show standard deviation from signal 203
 average spanning from 0.4 % and 1.29 %. Note that these er- 204
 rors are mainly due to slight variations of the X-ray intensity 205
 at the synchrotron beamline. The X-ray flux in a synchrotron 206
 is known to be a decaying function of time due to the lifetime 207
 limitations of the electrons within the storage ring. To overcome 208
 the problem, electrons are periodically injected into the storage 209
 ring to compensate beam losses and keep a constant photon flux 210
 at beamlines (cf. "top-up" operation). Since our measurements 211
 are realized between two successive "top-up", we numerically 212
 compensated the X-ray intensity decay in our data acquisition 213
 from a linear regression calculation. A linear regression being a 214
 first approximation of the real time-varying decay of the X-ray 215
 beam, residual intensity fluctuations are preserved and explain 216
 the harmonic fluctuations of the data points visible in Fig. 3(a). 217
 Therefore the offsets to the perfect repeatability imputed to our 218
 detection system are smaller than the values given in the figure 219

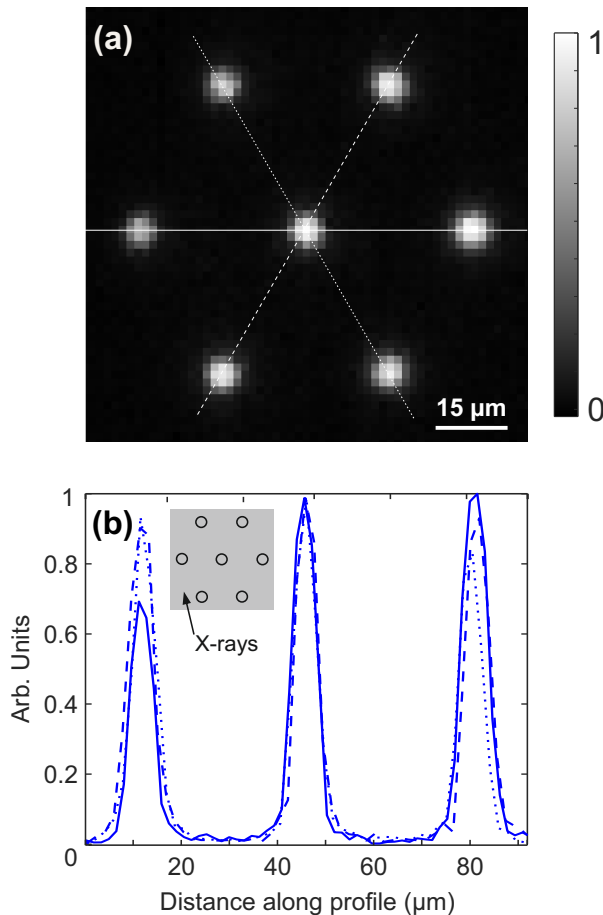


Fig. 2. (a) Optical image of the fiber output face when the pixel array is exposed to a $1 \times 1 \text{ mm}^2$ radiation field (see inset of (b)). (b) Intensity plots along the three white lines of (a).

inset. The linearity of the detector with regards to the deposited dose is assessed by accumulating the signals detected by each of its fiber-integrated pixel over 1, 3, 5, 10, 15, 20, 25, 30, 35 and 40 seconds of irradiation at a near-constant flux (see Fig. 3(b)). The linearity factor R across the pixel array exceeds 0.999.

To evidence potential spurious inter-pixel cross-talk in the overall detection process, the X-ray radiation is narrowed until exposing only one of the seven pixels of the fiber probe. To this end, the diaphragm diameter is decreased down to $35 \mu\text{m}$ and the resulting pinhole is centered with respect to a single pixel at the fiber detector. Fig. 4(a) reports an optical image of the output endface of the fiber when the tight X-ray pencil selectively irradiate the pixel at the center of the detection array. We see that only the exposed pixel delivers light to the camera via the multicore fiber, the neighboring detection channels remain unexcited. This is confirmed on the intensity plots of Fig. 4(b). Outside the fiber core coupled to the pixel under exposure, the detected intensity is at the level of the dark signal of the camera: inter-pixel cross-talk is therefore negligible.

Our fiber detector can operate under polychromatic X-ray radiations as well. This has been verified by testing the fiber system with a polychromatic radiation from a Cu-target source (20 kV, $40 \mu\text{A}$ / Bruker D8 DISCOVERY diffractometer). Figure 5 shows time traces simultaneously delivered by the seven pixels of the fiber probe upon exposure. At the beginning and at the end of the acquisition, the source shutter is closed to verify

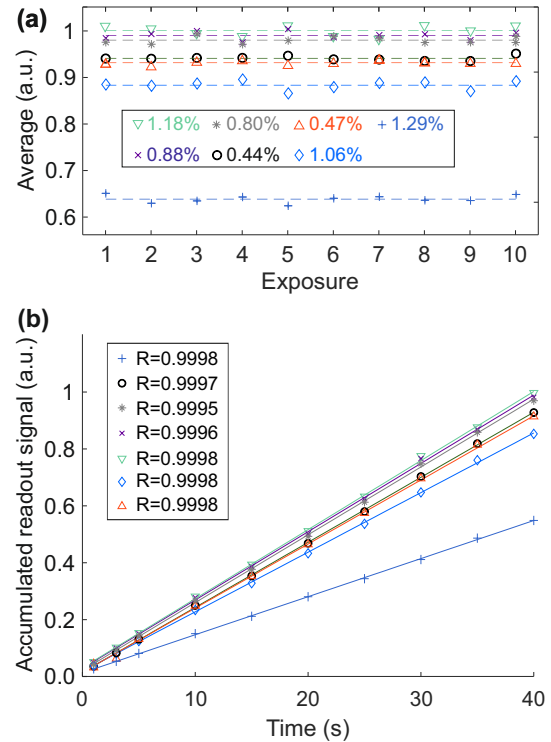


Fig. 3. (a) Repeatability of the multipixel detection system over ten successive exposures. (b) Linearity of the detector versus the exposure duration (i.e., accumulated dose).

that no spurious residual light (such as in-fiber coupled room light or scintillator afterglow) is detected by the system. We see that without X-rays, the afterglow generally observed with Eu-doped gadolinium oxysulfide [22] is here negligible. When the shutter is open (during 110 seconds), seven signals are simultaneously detected with a signal-to-noise ratio ranging from 30 to 42. Note that the signal-to-noise ratio can be enhanced by finding an optimum combination between tip shape and scintillator concentration within the photopolymer. All the above-studied detection properties and performances are also verified with this polychromatic source.

To conclude, we introduce the concept of a multi-pixel X-ray detector integrated at one endface of an individual multicore fiber. A seven-pixel array is demonstrated onto a narrow $125\text{-}\mu\text{m}$ diameter seven-core fiber, each pixel being engineered simultaneously on top of each fiber core by photolithography. The resulting imaging system shows good repeatability and linearity regarding the accumulated radiation dose and it is totally free from inter-pixel crosstalk. Such a fiber detector could be used to perform multi-point analysis of X-ray microbeams. This multipoint detection unit could also be seen as a building block of future ultracompact camera engineered from a bundle of multicore fibers. Being compact and flexible, such fiber camera systems would enable *in situ* or *in vivo* high resolution imaging in hard-to-reach locations. By leveraging the ubiquity of fiber-optics technology, this may represent new prospects in a broad range of scientific, medical, and industrial applications.

Funding.

Acknowledgments. Carlos Chacon, Miguel Suarez, Vahe Karakhanyan and Thierry Grosjean acknowledge financial support from the French Agency of Research (contract ANR-18-CE42-0016), the

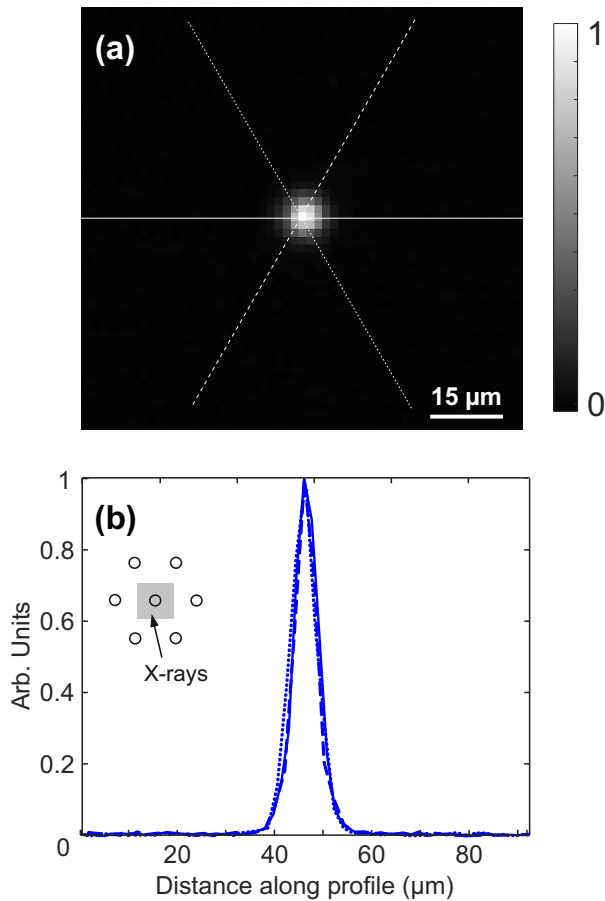


Fig. 4. (a) Optical image of the fiber output face when the pixel array is exposed to a $35 \times 35 \mu\text{m}^2$ radiation field centered with respect to the center pixel (see inset of (b)). (b) Intensity plots along the three white lines of (a).

218 SAYENS Agency, the EIPHI Graduate School (contract ANR-17-EURE-
219 0002) and the Region Bourgogne Franche-Comte. This study is also
220 partly supported by the French RENATECH network and its FEMTO-ST
221 technological facility.

222 **Disclosures.** The authors declare no conflicts of interest.

223 **Data availability.** Data underlying the results presented in this
224 paper are not publicly available at this time but may be obtained from
225 the authors upon reasonable request.

226 REFERENCES

- 227 1. S. O’Keeffe, D. McCarthy, P. Woulfe, M. Grattan, A. Hounsell, D. Sporea,
228 L. Mihai, I. Vata, G. Leen, and E. Lewis, *Br. J. Radiol.* **88**, 20140702
229 (2015).
- 230 2. L. Beaulieu and S. Beddar, *Phys. Med. & Biol.* **61**, R305 (2016).
- 231 3. L. Ding, Q. Wu, Q. Wang, Y. Li, R. M. Perks, and L. Zhao, *EJNMMI*
232 *physics* **7**, 1 (2020).
- 233 4. M. Jia, J. Wen, X. Pan, Z. Xin, F. Pang, L. He, and T. Wang, *Opt.*
234 *Express* **29**, 1210 (2021).
- 235 5. K. Chen, J. Ren, C. Zhao, F. Liao, D. Yuan, L. Lei, and Y. Zhao, *Opt.*
236 *Express* **29**, 22578 (2021).
- 237 6. M. Gonod, C. C. Avila, M. A. Suarez, J. Crouzilles, S. Laskri, J.-F.
238 Vinchant, L. Aubignac, and T. Grosjean, *Phys. Med. Biol.* **66**, 115016
239 (2021).
- 240 7. M. Gonod, M. A. Suarez, C. C. Avila, V. Karakhanyan, C. Eustache,
241 J. Crouzilles, S. Laskri, J.-F. Vinchant, L. Aubignac, and T. Grosjean,
242 *Phys. Med. Biol.* **67**, 245016 (2022).

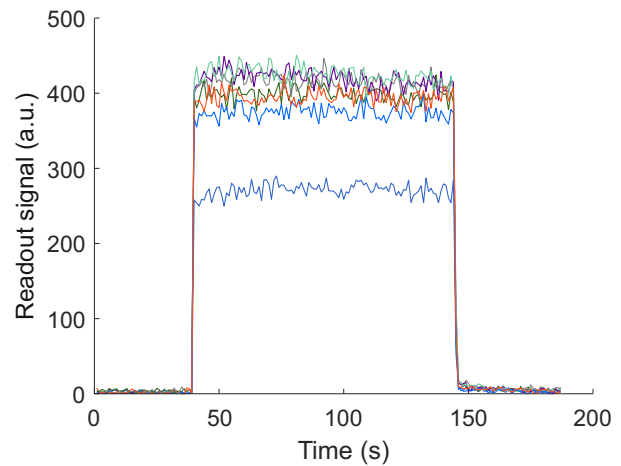


Fig. 5. Readout signal from the seven detection pixels upon a 110 s exposure to polychromatic X-rays from a Cu-target source. During the first and last 40 s of the acquisition, the source shutter is closed to assess the background (dark) signal of the system. When the radiation is activated, the SNR ranges from 30 and 42.

- 243 8. C. Penner, S. Usherovich, J. Niedermeier, C. Belanger-Champagne,
244 M. Trinczek, E. Paulssen, and C. Hoehr, *Electronics* **12** (2023).
- 245 9. L. Cartwright, N. Suchowerska, Y. Yin, J. Lambert, M. Haque, and
246 D. McKenzie, *Med. Phys.* **37**, 2247 (2010).
- 247 10. F. Therriault-Proulx, S. Beddar, and L. Beaulieu, *Med. Phys.* **40**.
- 248 11. H. M. Linares Rosales, P. Duguay-Drouin, L. Archambault, S. Beddar,
249 and L. Beaulieu, *Med. Phys.* **46**, 2412 (2019).
- 250 12. H. M. Linares Rosales, L. Archambault, S. Beddar, and L. Beaulieu,
251 *Med. Phys.* **47**, 4477 (2020).
- 252 13. Z. Zhao, Y. Dang, and M. Tang, “Advances in multicore fiber grating
253 sensors,” in *Photonics*, , vol. 9 (MDPI, 2022), p. 381.
- 254 14. Z. Zhao, M. Tang, and C. Lu, *Opto-Electronic Adv.* **3**, 190024 (2020).
- 255 15. M. Pisco and A. Cusano, *Sensors* **20**, 4705 (2020).
- 256 16. Y. Xiong and F. Xu, *Adv. Photonics* **2**, 064001 (2020).
- 257 17. C. Ecoffet, A. Espanet, and D. Lounnot, *Adv. Mater* **10**, 411 (1998).
- 258 18. R. Bachelot, C. Ecoffet, D. Deloeil, P. Royer, and D.-J. Lounnot, *Appl.*
259 *Opt.* **40**, 5860 (2001).
- 260 19. Z. Xie, Y. Lefier, M. A. Suarez, M. Mivelle, R. Salut, J.-M. Merolla, and
261 T. Grosjean, *Nano Lett.* **17**, 2152 (2017).
- 262 20. Z. Xie, H. Maradj, M.-A. Suarez, L. Viau, V. Moutarlier, C. Filiatre,
263 C. Fauquet, D. Tonneau, and T. Grosjean, *Opt. Lett.* **42**, 1361 (2017).
- 264 21. M. A. Suarez, T. Lim, L. Robillot, V. Maillot, T. Lihoreau, P. Bontemps,
265 L. Pazart, and T. Grosjean, *Opt. Express* **27**, 35588 (2019).
- 266 22. B. Ortega-Berlanga, L. Betancourt-Mendiola, C. del Angel-Olarte,
267 L. Hernández-Adame, S. Rosales-Mendoza, and G. Palestino, *Crystals*
268 **11** (2021).
- 269 23. Y. Hu, Z. Qin, Y. Ma, W. Zhao, W. Sun, D. Zhang, Z. Chen, B. Wang,
270 H. Tian, and E. Lewis, *Sens. Actuator A-Phys.* **269**, 188 (2018).
- 271 24. Z. Qin, Y. Hu, Y. Ma, W. Zhao, W. Sun, D. Zhang, Z. Chen, and E. Lewis,
272 *Opt. Express* **24**, 5172 (2016).
- 273 25. B. Lee, K. W. Jang, D. H. Cho, W. J. Yoo, G.-R. Tack, S.-C. Chung,
274 S. Kim, and H. Cho, *Nucl. Instrum. Meth. A* **579**, 344 (2007).
- 275 26. S. Law, N. Suchowerska, D. McKenzie, S. Fleming, and T. Lin, *Opt.*
276 *Lett.* **32**, 1205 (2007).